8. J. F. Partridge, B. Borgstrom, R. C. Allshire, *Genes Dev.* **14**, 783 (2000).
9. X. Bi, J. R. Broach, *Curr. Opin. Genet. Dev.* **11**, 199 (2001).
10. D. Donze, C. R. Adams, J. Rine, R. T. Kamakaka, *Genes Dev.* **13**, 698 (1999).
11. S. I. S. Grewal, A. J. S. Klar, *Genetics* **146**, 1221 (1997).
12. S. I. S. Grewal, *J. Cell. Physiol.* **184**, 311 (2000).
13. G. Thon, A. Cohen, A. J. S. Klar, *Genetics* **138**, 29 (1994).
14. N. Ayoub, I. Goldshmidt, A. Cohen, *Genetics* **152**, 495 (1999).
15. J. Nakayama, J. C. Rice, B. D. Strahl, C. D. Allis, S. I. S. Grewal, *Science* **292**, 110 (2001).
16. A. J. Bannister *et al.*, *Nature* **410**, 120 (2001).
17. Chromatin immunoprecipitations were performed essentially as described (*7, 8*). Fission yeast cells grown at 32°C in yeast extract adenine (YEA) medium (5×10^8 cells at 10^7 cells/ml for each reaction) were shifted to 18°C for 2 hours before 30-min fixation in 3% paraformaldehyde, and then were used to prepare soluble chromatin. Chromatin fractions were fragmented to ~0.5- to 0.8-kb DNA fragments before immunoprecipitation using antibodies to Swi6, H3 Lys^9-methyl, or H3 Lys^4-methyl. DNAs recovered from immunoprecipitated chromatin fractions or from whole-cell crude extracts were subjected to PCR analyses (94°C, 30 s; 55°C, 30 s; 72°C, 1 min; 30 cycles). PCR products were labeled by including 0.25 μl of [α-^{32}P]deoxycytidine triphosphate (10 mCi/ml) in each reaction; they were separated on a 4% polyacrylamide gel, and band intensities were quantified using a Fuji phosphoimager.
18. B. D. Strahl, C. D. Allis, *Nature* **403**, 41 (2000).
19. T. Jenuwein, C. D. Allis, *Science* **293**, 1074 (2001).
20. B. D. Strahl, R. Ohba, R. G. Cook, C. D. Allis, *Proc. Natl. Acad. Sci. U.S.A.* **96**, 14967 (1999).
21. K. Takahashi, E. S. Chen, M. Yanagida, *Science* **288**, 2215 (2000).
22. H. Wang *et al.*, *Science* **293**, 853 (2001); published online 31 May 2001 (10.1126/science.1060781).
23. Because of recombination block in the silent mating-type region, replacement of IR-L or IR-R elements with *kan*^{r} was performed in the *swi6* mutant background, which allows recombination in this region. The DNA fragment containing the marker gene flanked by sequence corresponding to the 5′ or 3′ sequence of the site of integration was gel-purified and used for transformation to construct IR-RΔ and IR-LΔ strains. PCR and Southern analyses were used to confirm replacements. Genetic crosses were used to obtain *swi6*$^+$ derivatives of the above strains. Deletions did not have a detectable effect on silencing of *ura4*$^+$ (*Kint2::ura4*$^+$) inserted at the *K*-region.
24. T. I. Gerasimova, K. Byrd, V. G. Corces, *Mol. Cell* **6**, 1025 (2000).
25. H. N. Cai, P. Shen, *Science* **291**, 493 (2001).
26. E. Muravyova *et al.*, *Science* **291**, 495 (2001).
27. J. Nakayama, S. I. S. Grewal, unpublished data.
28. G. Thon, A. J. S. Klar, *Genetics* **134**, 1045 (1993).
29. We thank J. Rice and E. Heard for comments on the manuscript, J. Nakayama for helpful discussions and boundary element sequences, and G. Xiao, Y. Tsukamoto, R. Rice, and M. A. Jelnick for technical help. Supported in part by a grant from Ellison Medical Foundation (S.I.S.G.) and by NIH grants GM59772 (S.I.S.G.) and GM53512 (C.D.A.).

6 July 2001; accepted 17 July 2001

Crystal Structure of a Neutralizing Human IgG Against HIV-1: A Template for Vaccine Design

Erica Ollmann Saphire,[1] Paul W. H. I. Parren,[2] Ralph Pantophlet,[2] Michael B. Zwick,[2] Garrett M. Morris,[1] Pauline M. Rudd,[4] Raymond A. Dwek,[4] Robyn L. Stanfield,[1] Dennis R. Burton,[1,2]* Ian A. Wilson[1,3]*

We present the crystal structure at 2.7 angstrom resolution of the human antibody IgG1 b12. Antibody b12 recognizes the CD4-binding site of human immunodeficiency virus–1 (HIV-1) gp120 and is one of only two known antibodies against gp120 capable of broad and potent neutralization of primary HIV-1 isolates. A key feature of the antibody-combining site is the protruding, finger-like long CDR H3 that can penetrate the recessed CD4-binding site of gp120. A docking model of b12 and gp120 reveals severe structural constraints that explain the extraordinary challenge in eliciting effective neutralizing antibodies similar to b12. The structure, together with mutagenesis studies, provides a rationale for the extensive cross-reactivity of b12 and a valuable framework for the design of HIV-1 vaccines capable of eliciting b12-like activity.

HIV-1 vaccine development is greatly hindered by the extreme difficulty in eliciting a neutralizing antibody response to the virus (*1–3*). However, three human monoclonal antibodies have been identified that can efficiently neutralize a broad array of primary isolates of HIV-1 in vitro (*4*) and can protect against viral challenge in vivo (*5–9*). Antibody 2F5 (*10*) reacts with gp41, whereas 2G12 (*11*) and b12 (*12*) react with independent epitopes on gp120. Elucidation of the epitopes recognized by these antibodies may offer valuable insights into the design of antigens capable of eliciting a protective antibody response.

Antibody b12 was identified from a combinatorial phage display library developed from bone marrow donated by a 31-year-old homosexual male who had been seropositive, but without symptoms, for 6 years (*12*). This antibody recognizes a highly conserved epitope overlapping the CD4-binding region of gp120, which accounts for its broad recognition of different HIV-1 isolates. Antibody b12 neutralizes about 75% of clade B primary viruses and a similar, or somewhat lesser, proportion of other clades (*12, 13*). In addition, b12 can protect hu-PBL-SCID mice (*5*) and macaques (*7*) from viral challenge. This combination of potency and broad specificity suggests that the b12 epitope on gp120 may be a particularly effective target for vaccine design.

The b12 IgG1κ was expressed in CHO cells, purified, and crystallized as previously described (*14*). The crystal structure of the intact IgG1 was determined at 2.7 Å resolution through an exhaustive molecular replacement (MR) search using more than 100 individual Fc and Fab search models (*14*). The highly mobile hinge regions connecting the Fabs to the Fc domains were interpretable after extensive rebuilding, refinement, and density modification (Table 1). Only three residues of the upper hinge of one heavy chain, seven residues of a frequently disordered surface loop of one Fab C_H1 domain (residues 128 to 135), and three COOH-terminal residues from one Fc are disordered.

The IgG structure is highly asymmetric (Fig. 1) and can be considered a "snapshot" of the broad range of conformations available in solution. The overall shape is between a Y and a T, with a 143° angle between the major axes of the two Fabs (*15*). The IgG spans 171 Å from the apex of one antigen-binding site to the other. The Fc region is twisted nearly perpendicularly to the planes of the Fabs and shifted some 32 Å from the central dyad relating the two Fabs, so that it packs into the space beneath only one of the Fabs (Fig. 1).

The hinge regions form extended structures with some conformational variation in torsion angles between the two chains, reflecting the different relative placement and environment of the two Fabs relative to the Fc domain. One upper hinge forms a spiral arrangement similar to a partially unwound helix; the other forms an extended turn as the polypeptide chain reverses direction to connect the Fab to the Fc. The core hinge region contains two adjacent pairs of cysteine residues, but only one disulfide is ob-

[1]Department of Molecular Biology, [2]Department of Immunology, [3]The Skaggs Institute for Chemical Biology, The Scripps Research Institute, 10550 North Torrey Pines Road, La Jolla, CA 92037, USA. [4]Department of Biochemistry, University of Oxford, The Oxford Glycobiology Institute, South Parks Road, Oxford OX1 3QU, UK.

*To whom correspondence should be addressed. E-mail: wilson@scripps.edu, burton@scripps.edu

Table 1. Structure determination of IgG1 b12. Data to 2.7 Å resolution were collected from a single cryocooled crystal at SSRL Beamline 7-1 on a MAR (MAR-Research) 30-cm area detector and processed with DENZO and SCALEPACK (*38*). Although the R_{sym} for the highest resolution shell is relatively high (62.6%), this shell contains useful information, because the I/σ is 2.4 and because inclusion of these reflections clearly improved the electron density maps. The structure was determined by molecular replacement (MR) using the software package AMoRe within the CCP4 suite (*39*) as described (*14*). Initial R_{cryst} and R_{free} values after MR and substitution of the b12 sequence were 0.37 and 0.44, respectively. The structure was refined in CNS (*40*) using a maximum likelihood target function and an initial overall anisotropic temperature factor correction. Multiple cycles of rebuilding in TOM/FRODO (*41*), refinement, as well as density modification in DM (*42*) by using a perturbation γ correction, dramatically clarified density and allowed construction of approximately 65 residues in the hinge, carbohydrate, and solvent-exposed regions. The overall average *B* value is 90 Å^2, reflecting the high solvent content of the crystals and interdomain flexibility of the IgG molecule. However, the electron density, with exception of the flexible hinge region and some solvent exposed loops, is absolutely clear and completely unambiguous. Water molecules were only built into highly ordered regions of the structure. *B* values for protein atoms in the vicinity of the incorporated water molecules ranged from 30 to 65 Å^2.

Parameter	Value
Data collection	
Space group	R32
Unit cell dimensions (Å)	$a = b = 271.3$, $c = 175.2$
Matthew's coefficient (V_M, Å^{3}Da^{-1})	4.1, 70% solvent
Resolution	30–2.7 Å
Total observations	187712 (8424)*
Unique reflections	63686 (3113)*
R_{sym} (%)	7.2 (62.6)*
Completeness (%)	94.4 (95.5)*
Redundancy	2.9 (2.7)*
I/σ	17.6 (2.4)*
Refinement	
Total residues	1331
Water molecules	71
Sugars	18
Refinement range (Å)	30–2.7
R_{cryst} (%)	22.5
R_{free} (%)	27.2
Bond length deviation (Å)	0.005
Bond angle deviation (°)	1.2
Residues in most favored regions (%) of Ramachandran plot	83.7
Residues in disallowed regions (%)	0.2†
Average *B* value, protein (Å^2)	90
Average *B* value, water (Å^2)	58
Average *B* value, carbohydrate (Å^2)	142

*Values for outer shell from 2.75 to 2.70 Å. †Val^{51} of both light chains. This residue exists in a well-defined γ turn in almost all antibody structures, but is designated by PROCHECK (*43*) as an outlier.

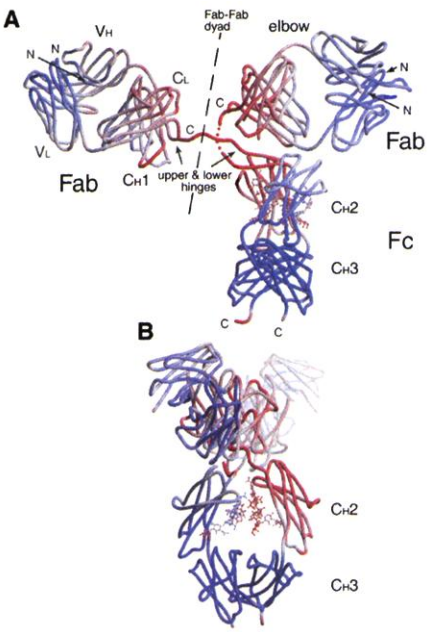

Fig. 1. Cα trace of the intact human IgG1 b12. The residues are colored by B value, with lower than average colored blue, average colored white, and higher than average colored red. (**A**) Front view showing the reach of the two Fabs and packing of the Fc domain underneath the right Fab. The hinge regions and one Fc C_H2 are characterized by the highest B values and greatest mobility. (**B**) Side view of the IgG [rotated 90° from (A)] demonstrating the near-perpendicular twist of the Fc relative to the Fabs. Carbohydrate chains form the contact between the C_H2 domains and are illustrated in ball-and-stick. Figure generated with Bobscript (*44*) and Raster3D (*45*). See (*46*) for an interactive image.

served in the electron density maps. The broken disulfide may be dynamic or may be a result of radiation damage, but probably has no functional importance, as only a single hinge disulfide is necessary for complement-mediated lysis and antibody-dependent cell-mediated cytotoxicity and phagocytosis (*16*).

Carbohydrate sequencing of b12 reveals two biantennary-branched oligosaccharide chains, but with branching fucose and terminal galactose residues in incomplete occupancy (*14*). This asymmetry is reflected in the electron density maps where one chain has both terminal galactose residues but lacks the fucose; the other incorporates the fucose but lacks the terminal galactose on the 1,3 arm.

Antibody b12 has a long CDR H3 (18 amino acids) that rises 15 Å above the surface of the antigen-binding site with a Trp residue at its apex (Fig. 2). A patch of acidic residues (*17*) along one face of this loop may help maintain the vertical projection through charge repulsion. This extended CDR H3 finger-like loop would allow the antibody to probe the recessed CD4-binding site of gp120; all members of a panel of 32 antibodies against the CD4-binding site developed from phage display have a similar length CDR H3 (*18*). To validate this notion, we designed a synthetic peptide to mimic the crystal structure of CDR H3. The peptide by itself is capable of viral neutralization when coupled to bovine serum albumin (BSA) (*19*) (Fig. 3).

Traditional views suggest that antigen-binding sites for antibodies against proteins are relatively flat. However, extended H3 loops are frequently seen in human antibodies directed against pathogens (*20*–*22*) that would allow them to access canyons and clefts on the viral surface (*23*). It is noteworthy that mouse antibodies do not normally exhibit such long CDR H3 loops, and indeed, few murine antibodies against the CD4-binding site have been described relative to the corresponding plethora of human antibodies of this specificity.

Ideally, we would prefer to dock our b12 structure onto an envelope gp120 trimer, as this is probably the relevant structure for neutralization. However, the only available gp120 structure is that of its monomeric core as a complex with CD4 and a Fab fragment (*24*). One interpretation of thermodynamic studies on recombinant monomeric gp120 is that CD4 binding might be accompanied by some structural rearrangement in gp120 (*25*). However, because structures of core gp120 from a primary isolate and a T cell line–adapted virus can be superimposed (*24*, *26*) and because earlier studies indicated that b12 and CD4 are sensitive to the same mutations in gp120, it is reasonable to use the CD4-bound core gp120 structure for generation of a docking model that can be tested by mutagenesis.

One hundred computational docking experiments were performed in parallel by using AutoDock (*27*). Each experiment used a 126 × 126 × 126 Å grid centered on gp120, each using 250,000 energy evaluations, and different, randomly selected initial orientations and translations of the b12 Fv. The best

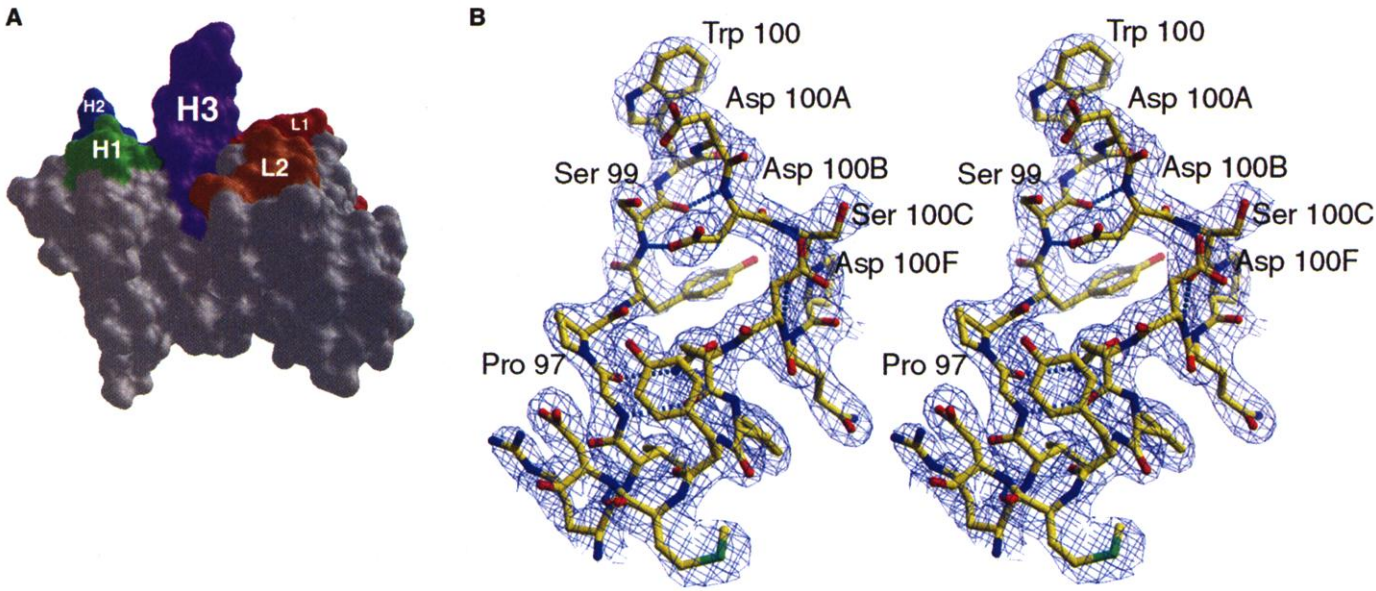

Fig. 2. Prominence of the CDR H3 finger-like loop in IgG1 b12. (**A**) Side view of the antigen-binding site of the Fv portion of b12. Contributions to the surface from each CDR are indicated. CDR H3 projects 15 Å above the other CDRs. (**B**) Stereo view of CDR H3 with surrounding final $2F_{obs} - F_{calc}$ electron density contoured at 2.0 σ. Trp^{100} is presented at the apex of the loop, and five intra-loop hydrogen bonds are indicated by dotted blue lines. The CDR H3 is unlikely to deform upon gp120 binding because of the presence of aromatic residues at the base and charge repulsion of the acidic patch on the inner face. In fact, four crystallographically distinct structures of the CDR H3 are identical [two on this symmetric IgG and two solved as Fab fragments in complex with a peptide (*47*)]. Molecular surfaces were calculated by using MSMS (*48*) and a 1.5 Å probe and visualized by using PMV (*49*). Density figure generated by using Bobscript (*44*) and Raster3D (*45*).

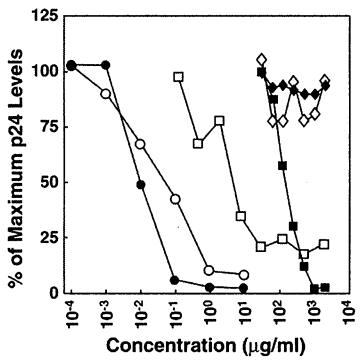

Fig. 3. Neutralization of HIV-1_{MN} and HIV-1_{HxB2} by IgG1 b12 and by a synthetic CDR H3 peptide. The peptide was designed as a CDR H3 loop mimic and coupled to BSA. A control peptide Gβ (American Peptide Co., Inc.) does not neutralize when coupled to BSA. HIV-1_{MN} and HIV-1_{HxB2} were neutralized by using H9 target cells and detection of p24 in ELISA as a reporter assay as described in (*5*). Filled circles, IgG1 b12 (MN); open circles, IgG1 b12 (HxB2); filled squares, CDR H3-BSA (MN); open squares, CDR H3-BSA (HxB2); filled diamonds, Gβ-BSA (MN); open diamonds, Gβ-BSA (HxB2).

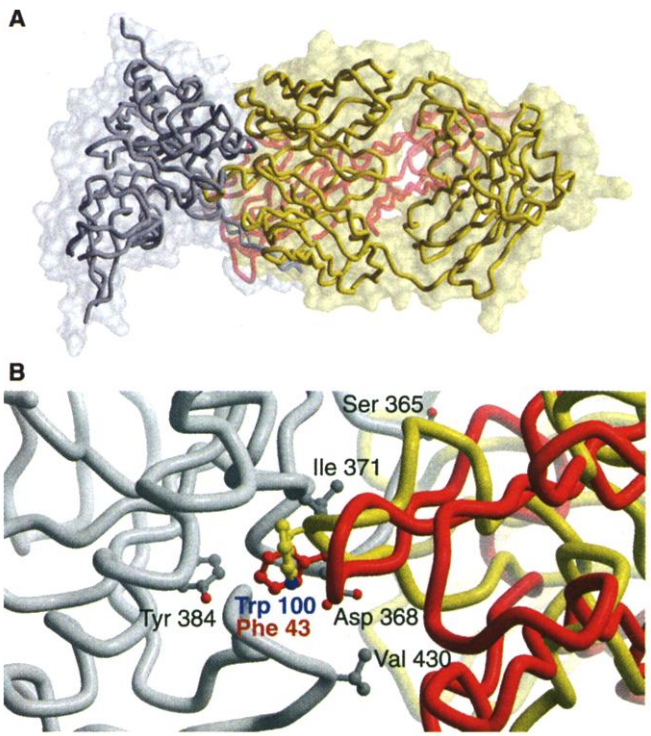

Fig. 4. Model of b12 interacting with gp120. (**A**) Comparison of Fab b12 docking onto gp120 with the CD4-gp120 crystal structure (*24*). Fab b12 is drawn as a Cα trace in yellow and gp120 in gray, showing the high complementarity of the gp120 and b12 structures, with their corresponding molecular surfaces outlined in the background. The placement of b12 overlaps with that of CD4 (red). (**B**) Close-up view of the docking. The b12 antibody presents Trp^{100} at the apex of the extended CDR H3 into the same pocket on gp120 that would be occupied by Phe^{43} of CD4 (red). Several gp120 residues (Ser^{365}, Asp^{368}, Ile^{371}, Tyr^{384}, and Val^{430}) that are important to b12 binding are illustrated in gray.

docking model has an energy of –24.7 kcal/mol, which is comparable to those obtained when docking CD4 onto gp120 in which AutoDock recreated the crystallized CD4-gp120 complex (*28*). This computational docking (Fig. 4A) arrives at a solution essentially identical to that first obtained manually, by using physical models generated from the b12 and gp120 coordinates.

The crystal structure of the gp120 complex (*24*, *26*) demonstrates that CD4 inserts a loop terminating in Phe^{43} into a polar pocket in gp120 in order to achieve complementarity (Fig. 4B). An antibody is twice as wide as CD4 (two immunoglobulin domains in width versus one). Thus, the imprint of a Fab onto the neutralizing face of gp120 will be extremely limited by geometric fit. The opening of the CD4-binding face of gp120 between the V1/V2 loop stem and constant region 4 (C4) is 35 Å wide, whereas the width of the Fab combining site is 31 Å. For gp120 in the envelope trimer, space for b12 binding in the lateral direction is bounded by the trimer interface and the 2G12 epitope, as b12 can bind native trimeric spikes (*29*), and also bind gp120

concurrently with antibody 2G12 (*30*). The docking shows that b12 may fit snugly onto gp120 by binding an epitope extending from the V1/V2 loop stem across the neutralizing face, with Trp^{100} at the tip of the H3 loop penetrating the Phe^{43} pocket (Fig. 4B). Trp^{100} is a crucial residue for b12 binding to gp120, as it is exclusively selected when CDR H3 residues are randomized (*31*). Further, mutation to Phe diminishes binding by 50% under conditions for which mutation to Ala, Val, or Ser diminishes binding by 85% (*32*).

IgG1 b12 and gp120 demonstrate complementary contact surfaces, like fingers fitting into a glove (Fig. 4A). The protruding ridge formed by Ser^{364} through Asp^{368} fits into a cleft between CDRs H3 and H2, and the protruding D loop of gp120 fits into a depression formed between CDRs H3, L1, and L3. In the docking model, approximately 2070 $Å^2$ of solvent-accessible surface is buried in the b12-gp120 interface (1030 $Å^2$ on gp120 and 1040 $Å^2$ on b12). The b12 interaction surface, like the footprint of CD4, is centered on the outer domain of gp120 with some additional contact extending to the V1/V2 loop stem, but with minimal contact to the inner domain.

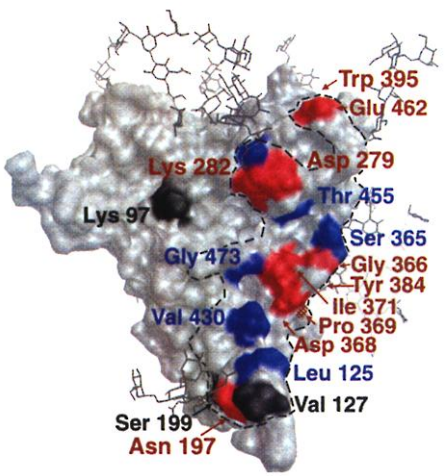

Fig. 5. Validation of the docking model of b12 onto gp120. Results of point mutations suggested by docking of b12 onto gp120 were mapped onto the gp120 surface. Mutation of residues in blue enhances b12 binding (>200% affinity relative to wild type); mutations in red diminish b12 binding (<50% relative affinity); and mutations in black have no significant effect (between 50 and 200% relative affinity). Most mutations are in the outer domain of gp120; see (*46*) for full characterization of mutants. The docking footprint of b12 on gp120 is outlined with a dashed black line. Variants of HIV-1 clade B isolates that escape neutralization by b12 have been generated in vitro (*50*) and in vivo (*51*). A common feature of these neutralization escape variants is the mutation of a proline at position 369, which strongly reduces b12 binding to gp120 in clade B isolates (*50*). Hence, Pro^{369} has been indicated with hatched red lines in this figure. Figure generated in PMV (*49*).

From this docking, a list of likely contact residues was generated. Alanine mutation of seventeen of these and additional neighboring residues supports the docking model (Fig. 5). In fact, several mutations enhance b12 binding, suggesting that b12, like CD4, may recognize gp120 through many main-chain contacts, allowing b12 to be relatively insensitive to side-chain variation.

The ability of b12 to neutralize primary viruses is associated with its ability to bind trimeric, as well as monomeric, gp120, whereas the other nonneutralizing CD4-binding site antibodies principally bind only monomeric gp120. Antibody b12 is also unique in its sensitivity to mutations associated with the V1/V2 loop (*29*) and, in particular, to changes in the V2 stem structure (*33*). In our model, the b12 Fab fits onto gp120 by contacting the inside face of the V1/V2 loop stem. We suggest that this mode of interaction angles the rest of the antibody bulk away from the trimer interface in an arrangement that permits attachment to the oligomeric spikes on the viral surface. Thus, the likely reason that antibody b12 is capable of potent neutralization of a broad array of isolates is that its interaction with the conserved CD4 epitope is mediated through many main-chain contacts and is angled in such a way that the antibody can access its epitope on the native viral surface.

Trimeric envelope spikes have three equivalent CD4-binding sites. Although the 170 Å reach of the IgG indicates that it could bivalently span two different spikes (*34*), b12 would probably not be able to bind simultaneously to two binding sites on the same trimeric spike. Nevertheless, the large mass (150 kD) of the IgG molecule compared with that of the envelope trimer is likely to block attachment of the virus to the target cell and/or fusion of viral and cell membranes, even at coating densities well below three IgG molecules per trimeric spike (*35*).

In conclusion, the structure of an intact human antibody capable of neutralizing a broad range of primary HIV-1 isolates illuminates the surface topography of the antigen-binding site. The highly extended CDR H3 is capable of accessing the vulnerable CD4-binding site of gp120 and may provide leads for antiviral compounds or peptides. Fine mapping of the b12 epitope also facilitates the design of minimized gp120 cores or peptidomimetics. Such structural information should provide new possibilities in the global effort to design an effective HIV-1 vaccine.

References and Notes:

1. R. Wyatt, J. Sodroski, *Science* **280**, 1884 (1998).
2. D. R. Burton, *Proc. Natl. Acad. Sci. U.S.A.* **94**, 10018 (1997).
3. P. W. H. I. Parren, J. P. Moore, D. R. Burton, Q. J. Sattentau, *AIDS* **13** (suppl. A), S137 (1999).
4. M. P. D'Souza, D. Livnat, J. A. Bradac, S. H. Bridges, *J. Infect. Dis.* **175**, 1056 (1997).
5. M. C. Gauduin *et al.*, *Nature Med.* **3**, 1389 (1997).
6. J. R. Mascola *et al.*, *Nature Med.* **6**, 207 (2000).
7. P. W. H. I. Parren *et al.*, *J. Virol.* **75**, 8340 (2001).
8. T. W. Baba *et al.*, *Nature Med.* **6**, 200 (2000).
9. J. R. Mascola *et al.*, *J. Virol.* **73**, 4009 (1999).
10. T. Muster *et al.*, *J. Virol.* **67**, 6642 (1993).
11. A. Trkola *et al.*, *J. Virol.* **70**, 1100 (1996).
12. D. R. Burton *et al.*, *Science* **266**, 1024 (1994).
13. A. Trkola *et al.*, *J. Virol.* **69**, 6609 (1995).
14. E. O. Saphire, P. W. H. I. Parren, C. F. Barbas, D. R. Burton, I. A. Wilson, *Acta Crystallogr.* **D57**, 168 (2001).
15. Definitions of axes used to quantify rotational and translational asymmetry. A central dyad was defined by the rotation axis that relates one Fab to the other Fab. One Fab is translated 16 Å from the other along the dyad (translation defined by the intersections of the Fab major axes with that dyad). The three axes within each domain (major, minor, and depth) are defined as follows: A major axis, extending from the hinge attachment point at the COOH-terminus to the center of the antigen-binding site was defined by the pseudo-dyad relating the C_H1 to C_L subdomains in the Fabs and the dyad relating the C_H3 subdomains in the Fc. The minor axis was defined as perpendicular to the major axis and extending across the flexible switch regions between the variable and constant domains of the Fabs (roughly across residues 107 of the light chain and 113 of the heavy chain) and across the switch region connecting the C_H2 to C_H3 domain of the Fc. The depth axes extend in the third dimension perpendicularly to both the major and minor axes. The 158° rotation of one Fab relative to the other refers to the rotation between the two depth axes of the two Fabs. Fab elbow angles are defined as the angle of intersection of the pseudo-dyad relating C_H1 and C_L with the pseudo-dyad relating V_H and V_L. The elbow angles (170°, 174°) differ slightly between the two Fabs. The Fc elbow angle, defined by the intersection of the dyad relating the C_H3 domains with the dyad relating the C_H2 domains, is 175°, revealing some asymmetry in the two halves of the Fc.
16. T. E. Michaelsen *et al.*, *Proc. Natl. Acad. Sci. U.S.A.* **91**, 9243 (1994).
17. Asp 100A, Asp 100B, Asp 100F, Ser 99, Ser 100C, and Tyr 100I. Alanine mutation of any of the three Asp residues along this face results in weaker binding to $gp120_{IIIB}$ (*32*).
18. All of the clones, with one exception, have a CDR H3 length of 18 to 22 residues (*21*), which is in marked contrast to the normal variation seen in other human antibodies (*36*). Antibodies to other HIV-1 epitopes have CDR H3 lengths ranging between 4 and 18 residues. The long length is not a function of their generation from a combinatorial library, because similar libraries of human antibodies against other pathogens display great variation in CDR length.
19. A synthetic peptide mimic of the CDR H3 was designed on the basis of the b12 crystal structure. The peptide extends from Ala^{93} to Trp^{103} and is linked at the base through native chemical ligation (*37*) and a Pro-Gly-Lys to promote type II β turn formation (sequence: C-PGK-ARVGPYSWDDSPQDNYYMDVW). The peptides were coupled to activated BSA (Pierce) through linkage with the cysteine residue at the base of the loop. Activity of the CDR H3 peptide was compared to that of b12 and of a control peptide similarly linked to BSA (GTP-binding peptide of sequence CEGNVRSRELAGHTGY; American Peptide Co.). The peptide neutralizes HIV-1_{MN} and HIV-1_{HxB2}. As expected, a higher concentration of the synthetic CDR H3 is required compared to the parental antibody that contains all six CDRs. HxB2 is a molecular clone of the HIV-1 strain IIIB. Single-letter abbreviations for the amino acids are as follows: A, Ala; C, Cys; D, Asp; E, Glu; F, Phe; G, Gly; H, His; I, Ile; K, Lys; L, Leu; M, Met; N, Asn; P, Pro; Q, Gln; R, Arg; S, Ser; T, Thr; V, Val; W, Trp; and Y, Tyr.
20. R. Kunert, F. Ruker, H. Katinger, *AIDS Res. Hum. Retrovir.* **14**, 1115 (1998).
21. C. F. Barbas *et al.*, *J. Mol. Biol.* **230**, 812 (1993).
22. P. P. Sanna, R. A. Williamson, A. De Logu, F. E. Bloom, D. R. Burton, *Proc. Natl. Acad. Sci. U.S.A.* **92**, 6439 (1995).
23. T. J. Smith, E. S. Chase, T. J. Schmidt, N. H. Olson, T. S. Baker, *Nature* **383**, 350 (1996).
24. P. D. Kwong *et al.*, *Nature* **393**, 648 (1998).

25. D. G. Myszka *et al.*, *Proc. Natl. Acad. Sci. U.S.A.* **97**, 9026 (2000).
26. P. D. Kwong *et al.*, *Structure Fold. Des.* **8**, 1329 (2000).
27. G. M. Morris *et al.*, *J. Comp. Chem.* **19**, 1639 (1998).
28. AutoDock 3.0.5 was used to perform all protein-protein docking experiments by using the Lamarckian Genetic Algorithm (*27*). AutoGrid chemical affinity and electrostatics maps were computed and centered on gp120 with 126 × 126 × 126 grid points at a spacing of 1 Å. As a test of the method, AutoDock was able to dock the D1 domain of CD4 onto gp120 to recreate the crystallized complex of CD4 and gp120 to within 0.5 Å root mean square (rms) deviation. For CD4-gp120 docking, correct solutions clustered together at about −21 kcal/mol, whereas the next lowest energy solutions were about −11 kcal/mol. In order to reduce the number of atoms in the large b12-gp120 docking experiment, we docked only the Fv domain instead of the intact IgG. The two lowest energy dockings could be ruled out because the antibody constant domains overlapped gp120 when the full antibody was reconstructed from the Fv fragment. The next four lowest energy dockings formed the largest cluster, and had a median rms deviation of 2.3 Å from the initial model generated by hand from geometric constraints. This initial model complex was solvated by a 5 Å shell of water molecules, and energy minimization performed by using the Discover 3 module of Insight II 2000 package (Molecular Simulations, San Diego, CA) and the CVFF force field for 100 iterations. This short minimization was enough to relieve any close contacts. Docking of the minimized structures resulted in a large 11-member cluster of solutions, with an average energy of −24.7 kcal/mol, unambiguously separated in energy from the remaining solutions.
29. P. Roben *et al.*, *J. Virol.* **68**, 4821 (1994).
30. J. P. Moore, J. Sodroski, *J. Virol.* **70**, 1863 (1996).
31. W. P. Yang *et al.*, *J. Mol. Biol.* **254**, 392 (1995).
32. M. B. Zwick *et al.*, unpublished data.
33. J. M. Binley *et al.*, *AIDS Res. Hum. Retrovir.* **14**, 191 (1998).
34. H. R. Gelderblom, E. H. Hausmann, M. Ozel, G. Pauli, M. A. Koch, *Virology* **156**, 171 (1987).
35. D. R. Burton, E. O. Saphire, P. W. H. I. Parren, *Curr. Top. Microbiol. Immunol.* **260**, 109 (2001).
36. I. Sanz, *J. Immunol.* **147**, 1720 (1991).
37. P. E. Dawson, T. W. Muir, I. Clark-Lewis, S. B. Kent, *Science* **266**, 776 (1994).
38. Z. Otwinowski, W. Minor, *Methods Enzymol.* **276**, 307 (1997).
39. J. Navaza, *Acta Crystallogr.* **A50**, 157 (1994).
40. A. T. Brünger *et al.*, *Acta Crystallogr.* **D54**, 905 (1998).
41. T. A. Jones, in *Computational Crystallography*, D. Sayre, Ed. (Oxford Univ. Press, Oxford, 1982), pp. 303–317.
42. K. D. Cowtan, P. Main, *Acta Crystallogr.* **D52**, 43 (1996).
43. R. A. Laskowski, M. W. MacArthur, D. S. Moss, J. M. Thornton, *J. Appl. Crystallogr.* **26**, 283 (1993).
44. R. M. Esnouf, *Acta Crystallogr.* **D55**, 938 (1999).
45. E. A. Merritt, D. J. Bacon, *Methods Enzymol.* **277**, 505 (1997).
46. Supplementary material is available in *Science* Online at www.sciencemag.org/cgi/content/full/293/5532/1155/DC1.
47. E.O.S., M.B.Z., A. Menendez, P.W.H.I.P., D.R.B., J. K. Scott, and I.A.W., unpublished observations.
48. M. F. Sanner, A. J. Olson, J. C. Spehner, *Biopolymers* **38**, 305 (1996).
49. M. F. Sanner, *J. Mol. Graph. Mod.* **17**, 57 (1999).
50. H. Mo *et al.*, *J. Virol.* **71**, 6869 (1997).
51. P. Poignard *et al.*, *Immunity* **10**, 431 (1999).
52. Supported by NIH Grants GM46192 (I.A.W.), AI40377 (P.W.H.I.P.), and AI33292 (D.R.B.). We are extremely grateful to the staff of the Stanford Synchrotron Radiation Laboratory (SSRL) Beamline 7-1 for assistance in data collection, M. Wormald of the Oxford Glycobiology Institute (UK) for discussions of carbohydrate torsion angles, A. de Vos of Genentech for human Fc coordinates, J. Sodroski of Harvard University for plasmid pSVIIIenv, V. Roberts for discussions of electrostatics and docking, P. Dawson for peptide synthesis, P. Poignard for help with gp120 mutagenesis, and M. Wang and A. Hessell for technical assistance. This is publication 13874-MB from The Scripps Research Institute. The IgG1 b12 coordinates and structure factors have been deposited into the Protein Databank (PDB accession code 1HZH) and are available from wilson@scripps.edu.

17 April 2001; accepted 18 June 2001

Enforcement of Temporal Fidelity in Pyramidal Cells by Somatic Feed-Forward Inhibition

Frédéric Pouille and Massimo Scanziani*

The temporal resolution of neuronal integration depends on the time window within which excitatory inputs summate to reach the threshold for spike generation. Here, we show that in rat hippocampal pyramidal cells this window is very narrow (less than 2 milliseconds). This narrowness results from the short delay with which disynaptic feed-forward inhibition follows monosynaptic excitation. Simultaneous somatic and dendritic recordings indicate that feed-forward inhibition is much stronger in the soma than in the dendrites, resulting in a broader integration window in the latter compartment. Thus, the subcellular partitioning of feed-forward inhibition enforces precise coincidence detection in the soma, while allowing dendrites to sum incoming activity over broader time windows.

At certain brain synapses, reliable transmission is ensured through large, rapidly rising, excitatory postsynaptic potentials (EPSPs), which are able to trigger a spike with little latency variation (*1*).

In hippocampal pyramidal cells (PCs), the small size of most unitary EPSPs requires that synaptic activity summate to reach the spike threshold (*2*). In principle, the relatively long membrane time constant of these neurons (*3*) may allow EPSPs to summate over large time windows. The occurrence of spikes would then reflect the average synaptic bombardment over time instead of being selectively time-locked to coincident synaptic activity. Thus, it is not known whether the timing of a spike in PCs reports the timing of the afferent activity triggering the spike (*4*–*6*). This issue can be addressed experimentally by determining the time window within which the activity of independent synaptic inputs must occur to trigger a spike.

We recorded from CA1 PCs in acute hippocampal slices from rat brains in cell-attached mode to avoid interfering with the intracellular ionic composition. Two stimulation electrodes were placed in the stratum radiatum at 300 to 600 μm on each side of the recorded neuron (*7*). Stimulation intensity was set so that when the two Schaffer collateral pathways were stimulated simultaneously, the PC fired a spike, detected as a capacitive current, in about 50% of the trials (threshold stimulation). The probability of spiking steeply decreased when one of the stimuli was shifted in time in 2.5- or 5-ms steps (Fig. 1A). A Gaussian fit of the data gave a SD of 1.4 ms (n = 9 cells).

We then blocked γ-aminobutyric acid A receptors ($GABA_AR$) with bicuculline (20 μM) or with the more selective antagonist SR95531 (3 μM) (*8*) and readjusted the stimulation intensity of both pathways to match the spiking probability observed under control conditions with simultaneous stimulation (51 ± 3% in control conditions versus 50 ± 5% in the presence of bicuculline, n = 5 cells; 62 ± 6% in control conditions versus 64 ± 11% in the presence of SR95531, n = 4 cells). This increased the delay between stimulus and spike (8.2 ± 0.6 ms in control conditions, 16.8 ± 1.2 ms in the presence of $GABA_AR$ antagonist; n = 9 cells).

$GABA_AR$ antagonists greatly prolonged the integration window (SD = 17.8 ms in bicuculline, n = 5 cells; SD = 15.6 ms in SR95531, n = 4 cells). In addition, although spikes triggered with simultaneous stimulation under control conditions showed submillisecond variability in spike delay (jitter), as described for intracellular current injections (*9*), in the presence of $GABA_AR$ antagonists the jitter increased almost threefold (the SD was 0.5 ms in control conditions versus 1.4 ms with $GABA_AR$ antagonists, n = 9 cells; Fig. 1B).

We monitored the underlying synaptic events using whole-cell recordings. In voltage-clamped cells, a stimulus elicited an excitatory postsynaptic current (EPSC)–inhibi-

Brain Research Institute, University of Zurich, Winterthurerstrasse 190, CH-8057 Zurich, Switzerland.

*To whom correspondence should be addressed. E-mail: massimo@hifo.unizh.ch